Atmos. Chem. Phys. Discuss., 11, 22857–22891, 2011
www.atmos-chem-phys-discuss.net/11/22857/2011/
doi:10.5194/acpd-11-22857-2011

Atmospheric Chemistry and Physics Discussions

Advances and limitations of atmospheric boundary layer observations with GPS occultation over Southeast Pacific Ocean

F. Xie[1,2], D. L. Wu[2,*], C. O. Ao[2], A. J. Mannucci[2], and E. R. Kursinski[3]

[1]Joint Institute for Regional Earth System Science and Engineering (JIFRESSE), University of California, Los Angeles, California, USA
[2]Jet Propulsion Laboratory, California Institute of Technology, Pasadena, California, USA
[3]Department of Atmospheric Sciences, University of Arizona, Tucson, Arizona, USA
[*]now at: NASA/Goddard Space Flight Center, Greenbelt, Maryland, USA

Received: 17 July 2011 – Accepted: 3 August 2011 – Published: 12 August 2011

Correspondence to: F. Xie (fxie@jifresse.ucla.edu)

Published by Copernicus Publications on behalf of the European Geosciences Union.

Abstract

The typical atmospheric boundary layer (ABL) over the southeast (SE) Pacific Ocean is featured with a strong temperature inversion and a sharp moisture gradient across the ABL top. The strong moisture and temperature gradients result in a sharp refractivity gradient that can be precisely detected by the Global Positioning System (GPS) radio occultation (RO) measurements. In this paper, the Constellation Observing System for Meteorology, Ionosphere and Climate (COSMIC) GPS RO soundings, radiosondes and the high-resolution ECMWF analysis over the SE Pacific are analyzed. COSMIC RO is able to detect a wide range of ABL height variations (1–2 km) as observed from the radiosondes. Whereas, the ECMWF analyses systematically underestimate ABL heights. The sharp refractivity gradient at the ABL top frequently exceeds the critical refraction (e.g., -157 N-unit km^{-1}) and becomes the so-called ducting condition, which results in systematic RO refractivity bias (or called N-bias) inside the ABL. Simulation study using refractivity profiles based on radiosondes reveals that the N-biases are significant and the magnitudes of biases are vertical resolution dependent. The N-bias is also the primary cause of the systematically smaller refractivity gradient (rarely exceeding -110 N-unit km^{-1}) at the ABL top from RO measurement. However, the N-bias seems not affect the ABL height detection. Instead, the very sharp refractivity gradient and the large RO bending angle due to ducting allow reliable detection of ABL height from GPS RO. The seasonal mean climatology of ABL heights derived from a nine-month composite of COSMIC RO soundings over the SE Pacific reveals significant differences from the ECMWF analysis. Both show the deepening of ABL height from the shallow stratocumulus near the coast to a much higher trade wind inversion further off the coast. However, COSMIC RO shows systematically higher ABL heights overall and reveals different locations of the minimum and maximum ABL heights as compared to the ECMWF analysis. The significantly decreasing number of COSMIC RO soundings at lower latitudes along with the lower percentage of RO soundings penetrating into the lowest 500 m above mean-sea-level (a.m.s.l.), result in

ACPD

11, 22857–22891, 2011

generally small sampling errors in the mean ABL climatology and will not affect the morphology of RO ABL height climatology. The difference of ABL height climatology between COSMIC RO and ECMWF analysis over SE Pacific is significant and requires further studies.

1 Introduction

The atmospheric boundary layer (ABL) over the southeast (SE) Pacific Ocean is characterized by a strong, shallow inversion layer. Persistent shallow stratocumulus (Sc) cloud decks trapped below the ABL inversion play an important role in cloud-climate feedback processes because of its radiative cooling effect (e.g., Randall et al., 1984; Slingo 1990; Klein and Hartmann 1993; Ma et al., 1996; Bony and Dufresne, 2005; Clement et al., 2009). Lack of understanding and observations of complicated ABL processes (e.g., cloud radiative cooling, entrainment, turbulent mixing, ocean-atmosphere coupling) leads to great model uncertainties in weather and climate predictions (e.g., Randall et al., 1998; Zeng et al., 2004; Palm et al., 2005; Jordan et al., 2010). Observations of thermodynamic structure of the ABL over the open oceans are limited in space and time to ground-based measurements over islands, ship soundings and several field campaigns. Conventional passive microwave or infrared satellite sounders do not have a sufficient vertical resolution to resolve ABL structures. The Cloud-Aerosol Lidar and Infrared Pathfinder Satellite Observations (CALIPSO) lidar can provide high precision ABL height, with little thermodynamic information and limited sampling.

As a promising technique for profiling the shallow ABL, Constellation Observing System for Meteorology Ionosphere and Climate (COSMIC) radio occultation (RO) observations (available since 2006) can measure ABL properties with global coverage, high vertical resolution (~200 m in the lower troposphere) and cloud-penetrating capability. Several studies have demonstrated the values of RO soundings in detecting the ABL height (e.g., Sokolovskiy et al., 2006, 2007; Ao et al., 2008; Basha and Ratnam, 2009). However, probing the ABL interior with RO remains to be challenging. One of the

ACPD
11, 22857–22891, 2011

critical problems is the systematic negative refractivity biases (N-bias) in RO sounding profiles, which is often pronounced over the subtropical eastern oceans (Xie et al., 2010), where the persistent sharp temperature and moisture gradient at the ABL top often results in the so-called ducting (or super-refraction) conditions (e.g., von Engeln and Teixeira, 2004; Lopez, 2009). In particular, over the SE Pacific, the overall quality and the scientific value of the RO soundings inside ABL are yet to be explored.

In this study, we analyze the quality of COSMIC RO soundings in the SE Pacific ABL by comparing the ABL top height measurements with those from the VAMOS Ocean-Cloud-Atmosphere-Land Study Regional Experiment (VOCALS-Rex) radiosonde (Wood et al., 2011) and the high-resolution European Centre for Medium-Range Weather Forecasts (ECMWF) analysis data. The paper is organized as follows: Sect. 2 describes the datasets used in this study, followed by methodology and validation results in Sect. 3; Sect. 4 compares ABL observations over the SE Pacific between parameters from COSMIC RO, VOCALS radiosondes and high-resolution ECMWF analysis; Sect. 5 present a seasonal mean of ABL top height from COSMIC RO and ECMWF analysis; Sect. 6 discusses advances and limitations of current RO soundings for ABL study; Finally, conclusions and future remarks are given in Sect. 7.

2 Data description

This study focuses on GPS RO boundary layer measurements over the SE Pacific (Fig. 1) where VOCALS-Rex field campaign took place during 20 October–1 December 2008 (Wood et al., 2011). COSMIC RO soundings and the launch locations of the radiosondes from NOAA research vessel (R/V *Ronald H. Brown*) are shown. A total of 213 radiosondes (10-m vertical sampling) were obtained at a 4-h interval. The COSMIC RO measurements are the retrievals from Jet Propulsion Laboratory (JPL), available at http://genesis.jpl.nasa.gov (e.g., Hajj et al., 2002; Ao et al., 2009). The refractivity is reported as a function of geometric height above mean-sea-level (a.m.s.l.), whereas the bending angle is reported as a function of impact parameter, which is the product

ACPD
11, 22857–22891, 2011

of refractive index and Earth's radius at the tangent point. The detailed description of GPS RO occultation technique has been described in earlier studies (e.g., Kursinski et al., 1997; Anthes et al., 2008 etc.). Although RO soundings could potentially achieve ~60 m vertical resolution (Goburnov, 2004), the resolution of JPL bending angle and refractivity profiles is limited by a 200 m filter applied in the standard retrieval. Since the marine ABL is the main focus of this paper, only RO profiles that penetrate below mean-sea-level = 0.5 km are used. This screening eliminates almost all RO profiles over the continents.

We also examine the high-resolution ECMWF global analysis data (TL799L91), which have a horizontal resolution of ~25 km (0.25° latitude × 0.25° longitude) with 91 vertical layers from the surface to 0.01 hPa (Bauer et al., 2006). The ECMWF six-hourly outputs have 17 unevenly-spaced layers below 800 hPa (~2 km), with denser sampling near the surface. The vertical resolution is roughly 200 m between 900 and 800 hPa, increased to 40 m near the surface.

The ECMWF assimilation has incorporated the COSMIC RO soundings in its analysis. However, ECMWF does not assimilate the RO profiles below the ducting layer at the ABL top (Poli et al., 2010), which is frequently seen in the analysis over subtropical eastern oceans, especially over SE Pacific (e.g., von Engeln and Teixeira, 2004; Lopez, 2009). Also the VOCALS radiosondes are not assimilated into the analysis. Therefore, to large extent, the RO, the radiosonde and the analysis data can be considered as independent measurements in the ABL.

3 Methodology and validation

Two important ABL parameters are analyzed here, ABL top height and refractivity gradient near the top. The ABL height is generally marked as a transition height with a strong temperature inversion and a sharp moisture gradient. It is a key parameter to characterize the ABL, which is determined by the vertical scale of turbulent eddies and controls flux exchanges among turbulent mixing, heat and moisture in the ABL. It also

ACPD
11, 22857–22891, 2011

depends on dynamic conditions of the underlining ocean surface and the free troposphere. The inversion strength, i.e., the temperature gradient across the thin transition layer (100–200 m thick) at the ABL top, is a measure of the stability of the transition layer. The inversion strength along with turbulent kinetic energy (TKE) controls the entrainment rate, a critical cloud dynamic parameter that determines the magnitude of warming and drying of ABL by mixing its air with free troposphere air (Lilly, 1968; Deardorff, 1976). The ABL inversion strength plays a critical role in evolution of cloud thickness and coverage (Wood and Bretherton, 2004; Wood and Hartmann, 2006). Although GPS RO cannot infer the ABL temperature inversion directly, the RO refractivity gradient depends strongly on both temperature and moisture gradients, and thus can be used as a valuable observational constraint to the ABL inversion strength and the ABL top entrainment rate.

3.1 Typical ABL structure over VOCALS region

Figure 2a shows a typical ABL temperature and humidity structure from radiosonde observation over the VOCAL region. The ABL top is well defined by separating a moist, well-mixed boundary layer from the dry free troposphere above. The stratocumulus cloud is trapped underneath the inversion base (at ~1.52 km) where the relative humidity (not shown) exceeds 94 % (Wang et al., 1999). A very interesting kink is seen in the radiosonde temperature profile at the cloud bottom (~1 km), showing a change in the temperature lapse rate from a nearly dry-adiabatic (~9.5 °C km^{-1}, a well-mixed ABL) to a less steeper saturated-adiabatic lapse rate (~4.3 °C km^{-1}) inside the cloud. The near-coincident ECMWF analysis profile (Fig. 2b) shows a significantly lower inversion base (i.e., cloud top height) at ~1.1 km with smoother transition across the ABL top in temperature and specific humidity. The reduced sharpness is likely due to the coarser vertical resolution in ECMWF analysis (~200 m vertical sampling). As expected, the small structures of the transition from dry-adiabatic to saturated-adiabatic in the radiosonde are not present in the ECMWF profiles.

ACPD
11, 22857–22891, 2011

Derived from atmospheric temperature, humidity and pressure of radiosonde and ECMWF data, the refractivity profile is a variable to be compared directly with GPS RO observations (Smith and Weintraub, 1953; Kursinski et al., 1997). It is important to note that the opposite changes in temperature and moisture across the ABL top lead to an enhanced decrease in refractivity (Fig. 2c). Assuming a spherically symmetrical atmosphere, one can further compute the bending angle profile as would be observed by GPS RO for a given radiosonde or ECMWF refractivity profile (Fig. 2d). The sharp refractivity gradient at the ABL top is mapped to a sharp increase in bending angle that is observed in the COSMIC RO measurements.

As seen in Fig. 2c, the COSMIC RO refractivity profile agrees well with the radiosonde at heights above the boundary inversion (~1.5 km). Below this level, however, there is a systematically negative bias in the RO refractivity profile. On the other hand, high-resolution COSMIC RO bending (5-m smoothed) shows a sharp increase in bending angle at around 3 km (in impact height) closely matching the simulated radiosonde bending. The peak bending corresponds to the sharp refractivity gradient at the ABL top. Whereas, the standard RO bending angle (applied the 200-m vertical smoothing) shows a significantly lower and smaller peak bending angle.

Several studies have utilized such features in RO refractivity profile for detecting ABL height by locating the height of maximum refractivity gradient (MRG) in GPS RO profiles (e.g., Sokolovskiy et al., 2006; Ao et al., 2008; Basha and Ratnam, 2009). For a well-defined ABL (e.g., over VOCALS region), the refractivity gradient method is consistent with other conventional definitions (e.g., gradient method based on temperature or humidity profiles) (Basha and Ratnam, 2009; Seidel et al., 2010, von Engeln and Teixeira, 2011). However, over the region where the ABL transition layer do not have a sharp vertical gradient (e.g., the deep convection zone), this method could become problematic, giving significant discrepancies among ABL height definitions (e.g., von Engeln and Teixeira, 2011). In this paper, we choose the MRG method and define the ABL height as the altitude where the refractivity gradient reaches its most negative value anywhere below 5 km. Note that the three datasets are associated with different

ACPD
11, 22857–22891, 2011

vertical resolution: radiosonde (10 m), RO (~200 m) and ECMWF (varying from ~40 to ~200 m). To ensure the same ABL height quality derived with MRG method, we interpolate RO and ECMWF refractivity profiles (cubic-spline) on a 10 m vertical grid before the gradient calculation. RO shows a reasonably good agreement with radiosonde in ABL height with a negative bias of (90 m), while ECMWF analysis has a larger negative bias of ~200 m (Fig. 2c).

Given the simulated radiosonde bending angle profile, the refractivity profile can be derived (dotted-line in Fig. 2c) following the standard RO Abel retrieval process (e.g., Fjeldbo et al., 1971) The retrieved refractivity profile is also negatively biased as compared to the radiosonde refractivity. The negative bias is caused by the so-call ducting phenomenon (or super-refraction, i.e., maximum refractivity gradient exceed the critical refraction, -157 N-unit km^{-1}) at the top of the ABL where solutions to the Abel inversion problem become non-unique (Sokolovskiy, 2003; Ao et al., 2003; Xie, et al., 2006, 2010). In this example, the COSMIC RO refractivity closely matches the Abel-retrieved radiosonde refractivity profile, which suggests the negative bias in refractivity be primarily due to ducting. Additional negative biases of the RO refractivity profile, relative to the radiosonde Abel profile, could be due to other factors such as the space and time difference between RO and the radiosonde (~268 km, ~1 h) or the horizontal inhomogeneity of the atmosphere.

3.2 ABL height comparisons

Out of total 190 radiosonde profiles during the VOCALS field campaign in 15° S–25° S, 70° W–86° W, only 25 are found to be near-coincident with 120 quality-screened RO profiles. The criteria for the collocated profiles are within 3 h in time and 300 km in space. Figure 3a compares the ABL heights for the 25 matched cases (mean time difference = 1.5 h; mean-distance = 226 km), and a low bias (~200 m) is evident in the RO measurements. The correlation is ~0.69 with a standard deviation of ~230 m. The limited number of near-coincident cases and the relatively large space/time difference between RO and the radiosondes could contribute to the ABL height difference. The

ACPD
11, 22857–22891, 2011

radiosonde-ECMWF analysis (190 soundings) comparison, as shown in Fig. 3b, yields a low bias in the ECMWF analysis. The correlation is lower (~0.54) but with a smaller standard deviation of ~70 m. The negative bias in ABL height in ECMWF analysis is consistent with previous studies (e.g., Bretherton et al., 2004; von Engeln and Teixeira, 2011).

4 Atmospheric boundary layer over southeast Pacific Ocean

The short-period VOCALS campaign and the relatively sparse sampling of COSMIC RO soundings make it difficult to find a large number of coincident pairs. COSMIC RO has a random sampling pattern especially in the zonal direction (see details in Sect. 5), whereas radiosondes and ECMWF analysis have relatively uniform and dense sampling over the campaign area. An alternative approach is to evaluate ABL parameters through their PDF (probability density function or histogram) using all available data sets over the region of interest. These PDFs can also yield differences among COSMIC RO, radiosondes and ECMWF analysis.

4.1 ABL height comparisons

In this comparison the ABL heights are first derived from the refractivity profiles using the MRG method, and then sorted into 100 m bins between the surface and 4 km. The PDF in each bin, i.e., the number normalized by the bin size and the total number of observations in the 0–4 km height range. The PDF of the ABL heights for the 25 radiosondes (100-m smoothing), the near-coincident COSMIC RO soundings as well as the ECMWF analysis are shown in Fig. 4a. The PDF of COSMIC RO shows a better agreement with radiosonde than ECMWF. Both RO and radiosonde data show the maximum frequency of ABL height at ~1.5 km and exhibit the similar width of distribution. The ECMWF analysis, however, shows peak frequency of ABL heights at a much lower altitude (~1.1 km) and shifts the PDF to lower values.

ACPD
11, 22857–22891, 2011

A reduced vertical resolution results in a decrease in the vertical refractivity gradient and thus affects the ABL height derived from the MRG method. Figure 4b shows the PDF of the ABL heights for the 190 radiosondes (between 15° S and 25° S) after applying three vertical smoothing levels (100, 200 and 300 m). The ABL height at peak frequency (~1.3 km) does not change due to different level of smoothing. The 200-m smoothing result is almost identical to the 100-m smoothing. While the 300-m smoothing does reduce the peak frequency of ABL height at 1.3 km, but the overall shape (e.g., the width) of the PDF is maintained. This is because the ABL top is very well-defined, marked by the dominant sharp gradient across the ABL top in the lower troposphere, and is less sensitive to the smoothing. All three curves show the majority of ABL heights varying from 0.8 km to 2.1 km. On the other hand, the near-coincident ECMWF analysis (190 profiles, mean time difference = 1.5 h; mean-distance = 85 km) shows lower ABL height (1.1 km) at its peak occurrence frequency, which is very similar to Fig. 4a. Again, ECMWF analysis shows systematically lower ABL heights (by ~200 m at peak frequency), compared to the near-coincident radiosondes. This lower ABL height bias in ECMWF is consistent with the scatter plot in Fig. 3b.

We also compute the PDF of ABL heights from COSMIC RO soundings and the near-coincident ECMWF analysis (70 profiles, mean time difference = 1.5 h; mean-distance = 130 km) over the region (latitudes: 20° S–25° S, and longitudes: 70° W–86° W) during VOCALS campaign period. COSMIC RO soundings show the peak frequency of ABL height at 1.3 km, whereas the ECMWF analysis shows systematically lower ABL heights with a peak occurrence frequency at 1.1 km as seen in Fig. 4a, b. RO soundings are capable to resolve higher ABL with realistic range of ABL heights variation (0.9 km to 2.1 km) as revealed by the radiosondes (Fig. 4b). On the other hand, the ECMWF analysis systematically underestimates the ABL heights and shows limited capability of correctly reproducing the ABL height variations.

ACPD
11, 22857–22891, 2011

4.2 Maximum refractivity gradient (MRG) at the ABL top

Sharp temperature inversion and drop in moisture both contribute to the large gradient of refractivity across the ABL top. Note that the inversion strength is an important ABL parameter that measures the stability of the transition layer and controls the moisture and momentum fluxes exchange between the boundary layer and the free troposphere. It also strongly affects the cloud-top entrainment rate and evolution of stratocumulus clouds below the inversion (Wood and Bretherton, 2004). The refractivity gradient measurement, therefore, is important for understanding the cloud-top entrainment and other ABL processes.

In this section we investigate the PDF of MRG at the ABL height using the near-coincident pairs of radiosondes, ECMWF analysis and COSMIC RO as shown in Fig. 4b and c. To account for the large range of MRG values, we take the logarithm of the absolute value of MRG to base 10, and calculate the PDF with even bin size of 0.2 from 0 to 3. These bins are later converted back to the corresponding MRG from -1 to -1000 (N-unit km^{-1}) in linear scale. Again, the PDF measures the number of occurrences within each bin normalized by the total number of observations and by the bin size.

As expected, the refractivity gradient at the ABL top, or MRG value, depends on the vertical resolution of measurements. Lower vertical resolution leads to a smaller gradient. When the MRG is larger (more negative) than the critical refraction (-157 N-unit km^{-1}) the ducting condition occurs. With the original 10 m sampling, the MRG values of the radiosondes (190 profiles) vary from -200 to -1000 (N-unit km^{-1}). To investigate the smoothing effect on the MRG, we apply different smoothing lengths on the radiosonde data, and Fig. 5a shows the PDF of MRG for the radiosondes and the near-coincident ECMWF. The PDF peak shifts to a smaller MRG value when the smoothing length increases. With the 100-m and 200-m vertical smoothing, the radiosondes still show ~100 % ducting (i.e., MRG exceed critical refraction as indicated by the vertical dashed-line). The 100-m smoothing shows a peak PDF at -420 N-unit km^{-1}, which is

ACPD
11, 22857–22891, 2011

a very steep gradient that is rarely produced in global numerical models. At the 500-m smoothing, most radiosonde profiles are deprived of ducting layer.

On the other hand, the near-coincident ECMWF analysis (with ∼200 m vertical sampling) shows much broader range of MRG variations (−70 to −400) that don't match either PDF of the radiosndes with 200-m or 300-m smoothing. The MRG of ECMWF reaches around −200 N-unit km^{-1} at peak frequency, which is close to the radiosonde with 300-m smoothing. But it also shows much higher frequency of stronger gradient (< −240) as compared with radiosondes with 300-m smoothing. The large discrepancy between the near-coincident ECMWF analysis and the radiosonde with various vertical-smoothing levels could not be simply explained by the limited vertical resolution in the ECMWF model. Instead, it could imply some deficiency in the model physics to reproduce correct distribution of the MRG at the ABL top.

Similarly, the PDF of the MRG for COSMIC RO soundings over region (20° S–25° S, 70° W–86° W) is plotted along with the near-coincident ECMWF analysis (Fig. 5b). The ECMWF analysis shows similar PDF as Fig. 5a, but shows a slightly higher frequency for lower MRG, which could be related to less sharp inversion at higher latitudes toward the south. On the other hand, the RO measurements significantly underestimate the MRG. The MRG tends to saturate at ∼ −110 N-unit km^{-1}, which is much smaller than the critical refraction (−157 N-unit km^{-1}).

The radiosondes confirm the prevalence of a ducting layer at the ABL top over the VOCAL region. In the presence of ducting, the standard RO refractivity retrieval becomes a non-unique inversion problem (Sokolovskiy, 2003; Xie et al., 2006). With the assumption of 1-D atmosphere with horizontally extended ducting layer at the ABL top, the standard RO refractivity retrieval will have the MRG exactly equal to critical refraction (−157 N-unit km^{-1}), no matter how much the MRG exceeding the critical refraction in the real atmosphere.

The delta function like PDF of RO MRG in Fig. 5b implies the dominant presence of ducting, which leads to the convergence of the MRG (saturated) to the critical refraction threshold in RO soundings. However, the less sharp refractivity gradients (e.g.,

ACPD
11, 22857–22891, 2011

-110 N-unit km^{-1}) than the critical refraction (-157 N-unit km^{-1}) in COSMIC RO soundings is partially due to the vertical smoothing (~200-m) applied in the standard retrieval process. Moreover, the horizontal inhomogeneity in the atmosphere can introduce extra smoothing effects (e.g., Ao, 2007) but requires further investigation. Therefore, the systemically smaller MRG in COSMIC RO soundings should be primarily caused by ducting but not due to the lack of vertical resolution.

4.3 Refractivity bias (N-bias) due to ducting in RO soundings

The VOCALS radiosondes and ECMWF analysis confirm a wide-spread ducting layer at the top of the ABL over the SE Pacific (Fig. 5). The ducting layer has a profound impact on the propagation of radio waves and could result in systematically negative biases (or called N-bias) in RO refractivity retrievals (Sokolovskiy, 2003; Ao et al., 2003 and Xie et al., 2006), which results from the non-unique Abel inversion problem with details described in Xie et al. (2006). Xie et al. (2010) reveal the large N-biases in GPS RO soundings as compared with ECMWF analysis over subtropical eastern oceans across the globe, including the SE Pacific. The regions with significant N-biases are highly correlated with the area where elevated ducting prevails (von Engeln and Teixeira, 2004; Lopez, 2009).

Here we investigate the PDF of the N-bias caused by ducting using a simple two-step geometric-optics model. Based on the VOCALS radiosonde and ECMWF refractivity profiles, we conducted a two-step GO simulation: (1) a forward operator to compute the bending angle given a 1-D atmosphere represented by one refractivity profile; and (2) an inverse operator, or Abel inversion, which compute the refractivity profile by integrating the bending angle profile through the standard Abel-inversion (e.g., Xie et al., 2006). In the absence of ducting, the Abel-retrieved refractivity profile will be identical to the input refractivity profile and introduce no bias. However, in the presence of ducting, the Abel-retrieved refractivity profile will exhibit negative bias inside the ABL. The solely ducting-induced N-bias (in percentile) is defined as $(N_{\text{retrieval}} - N_{\text{input}})/N_{\text{input}} \cdot 100$.

ACPD
11, 22857–22891, 2011

The maximum N-bias of each simulated profile is generally near the top of ducting layer, i.e., the ABL top. Such simulations are applied on all radiosonde and ECMWF profiles. We then bin the N-biases from −20 % to 0 with a 2 % interval. The PDF of the N-bias is then normalized by the total number of observations and the bin size.

As shown in Xie et al. (2006), the maximum N-bias introduced by ducting is linearly proportional to the refractivity gradient at the ABL top (and thus is vertical resolution dependent. In the model simulations we compute the N-bias from the radiosonde data with various vertical-smoothing lengths. Fig. 6 shows the PDF of N-bias for radiosonde (with various smoothing) and ECMWF data. Consistent with the results in Fig. 5a, the radiosonde profiles with the 100-m and 200-m smoothing preserve the ducting and the peak frequency of maximum N-bias is as large as −12 % and −8 %, respectively. With further smoothing, the N-bias reduces to nearly zero bias. At the 500-m smoothing, most profiles have zero bias, since the MRG rarely exceed critical refraction at this level of smoothing. On the other hand, the PDF of the N-bias due to ducting in ECMWF is closest to the radiosonde result at the 300-m smoothing, but with a broader spread.

5 Seasonal mean ABL height climatology

It has been shown above that COSMIC RO is capable to detect the ABL top height from the sharp refractivity gradient despite the N-bias of RO profiles inside the ABL due to ducting. We further generate a three-month (September to November) ABL height composite using the aforementioned MRG method for COSMIC RO soundings over the SE Pacific region (0° ∼ 50° S and 70° W ∼ 140° W) in 2007–2009. The same method is also applied to ECMWF analysis (down-sampled to 1° latitude × 1° longitude spatial resolution) profiles in the region.

Deepening of the ABL depth westward off the coast is clearly evident in both COSMIC RO and ECMWF data (Fig. 7). COSMIC RO shows an overall deeper ABL and significant different pattern as compare to the ECMWF. A dipole feature in ABL heights is seen in COSMIC RO, i.e., a minimum ABL height (∼1.2 km) centered at (20° S, 75° W)

ACPD
11, 22857–22891, 2011

just off the coast of Peru and Chile border; and a maximum ABL height (~2.2 km) centered at (15° S, 130° W). COSMIC RO also shows the deepening of ABL structures westward off the coast from ~70° W all the way to the maximum at 130° W within the latitudes between ~8° S and ~25° S. The ABL heights increase steadily along 20° S with a relative steep slope of ~30 m 100 km^{-1} westward from ~80° W to ~90° W. The slope decreases significantly further westward to be ~10 m 100 km^{-1} between 100° W and 120° W. Interestingly, COSMIC also show rather inhomogeneous ABL height in the meridional direction, which is introduced by a "tongue" of low ABL heights extended northwestward from a local minimum close to the coast at (20° S, 75° W).

Although ECMWF analysis shows systematically shallower ABL height, a similar dipole feature, i.e., a minimum (less than 0.8 km) centered at (30° S, 72° W) and a maximum (~1.7 km) centered at (15° S, 115° W), is similar to what is observed from COSMIC RO. The deepening of the ABL (at 20° S) westward from ~75° W up to ~100° W is also seen in the ECMWF analysis with a same slope of ~30 m 100 km^{-1} between 75° W and 90° W as seen in COSMIC and a less steep slope further westward of 90° W before reaching the maximum ABL height. It is also interesting to note that, ECMWF analysis shows rather homogeneous ABL heights in meridional direction between ~8° S and 30° S from near the coast to the ~100° W, which is rather different from COSMIC RO.

The VOCALS radiosonde observations are too sparse to produce a map, but along 20° S (from 25 October to 1 November 2008) they also show the increasing of ABL height (based on MRG method) from 1.32 km (median value) at 75° W to ~1.57 km at 85° W along 20° S latitude, which is consistent with the airplane cloud radar measurements of cloud top height during VOCALS campaign (Fig. 2 in Bretherton et al., 2010). The one-month mean ABL height from radiosondes agrees better with the mean climatology in COSMIC RO (Fig. 7a) than ECMWF. The slope of ABL height is ~25 m 100 km^{-1} that is slightly less than COSMIC and ECMWF analysis.

A similar pattern of the ABL height variations with comparable magnitude is shown in the standard deviation plots in Fig. 7c and d. The ABL height variations tend to be smaller over stratocumulus region close to the coast with a local minimum at (18° S,

ACPD
11, 22857–22891, 2011

85° W) in COSMIC and at slightly northward for ECMWF analysis at (15° S, 90° W). The variations increase westward and in meridional directions. A local maximum in ECMWF (~0.8 km) is clearly seen at ~130° W in between 10° S and 25° S. COSMIC shows a slightly smaller maximum variance at the similar location. Large variances in ABL height are both seen in COSMIC RO and ECMWF analysis between 40° S and 50° S, where the storm track are located. COSMIC RO also shows large variation of ABL heights close to equator (0–5° S), which is likely due to the limited sampling of RO soundings close to the equator as shown in Fig. 8. Also note that the frequent convection in the tropics and the storm track at ~50° S generally leads to less well-defined ABL top, which will result in challenges of applying the simple MRG method to detect the ABL heights.

COSMIC RO has a relatively denser sampling per unit area at higher latitudes and it is important to understand the sampling errors in the ABL height climatology due to the inhomogeneous sampling of COSMIC RO in the meridional direction. As shown in Fig. 8a (shaded), during the total of 9-month study period, the sampling is rather homogeneous in zonal direction. The number of sampling within each 500 × 500 km area is ~160 profiles at 40° S and gradually reduces to a minimum of ~50 profiles from 10° S to the equator. Moreover, not all the RO profiles penetrate below 500 m above the mean-sea-level. The percentage of RO that penetrate into the lowest 500 m tends to be lower in the tropics than at higher latitudes (contours in Fig. 8a). For example, only about 20–30 % RO profiles penetrate deep into the lowest 500 m a.m.s.l. close to equator (0–10° S), whereas the penetration rate increases at higher latitude and reach over 60 % at ~50° S. Note that the penetration rate is rather homogeneous in zonal direction except slightly reduction in the grids close to the continent. This is artificial effect because the penetration requirement used for this study is reference to the mean-sea-level (i.e., RO profiles with the minimum altitude below 500 m a.m.s.l.), which eliminates most profiles over the continent due to the topography and artificially reduces the penetration rate.

ACPD
11, 22857–22891, 2011

To estimate potential sampling error with COSMIC RO, we sample the ECMWF analysis at the RO sounding locations for the study period and create a sub-sampled ABL height climatology (not shown). The difference between the full and sub-sampled ABL height climatology reveal the sampling errors (Fig. 8b). The sampling errors are generally less than 100 m and become larger at three major locations, i.e., negative errors in ABL heights up to −500 m close to (10° S, 140° W), and smaller positive errors of ∼100–200 m close to 130° W and 75° W at 35° S latitude. Therefore, the limited RO sampling results in generally small errors in ABL height and will not affect the general morphology of the ABL height climatology as shown in Fig. 7a.

6 Discussions

Over the SE Pacific, the cool SST along with the large-scale subsidence in the free troposphere lead to a well-defined ABL with a strong temperature inversion and a sharp moisture drop across the ABL top. Such a thin transition layer introduces a very sharp refractivity gradient and thus result in a large bending angle in RO signals, which can be precisely detected by the high-resolution GPS RO soundings. However, there are some limitations in GPS RO for ABL studies, which are discussed in the following.

6.1 Ducting effect on GPS RO

The sharp refractivity gradient at the ABL top over the VOCALS region often exceeds the critical refraction threshold (i.e., −157 N-unit km^{-1}) and results in ducting condition (also referred as super-refraction). The refractivity gradient is dominated by the moisture gradient in the tropics and subtropics (von Engeln and Teixeira, 2005; Ao, 2007). At ∼1 km altitude, a mere -2.5×10^{-2} g kg^{-1} m^{-1} in specific humidity will lead to ducting condition. Nearly all the VOCALS radiosonde profiles (between 15° S and 25° S) meet the ducting condition even with the 100-meter smoothing. The mean specific humidity gradient at the ABL top of these profiles is as large as -5.7×10^{-2} g kg^{-1} m^{-1} with a standard deviation of 2.8×10^{-2} g kg^{-1} m^{-1}.

ACPD
11, 22857–22891, 2011

A horizontally extended ducting layer results in a sharp increase in RO bending at the ABL top, which becomes infinite large (a singularity) in geometric optics simulation (Sokolovskiy, 2003). By applying the standard Abel retrieval (i.e., integrating through the infinite bending), the refractivity retrieval based on the spherically symmetric atmosphere assumption produces a maximum refractivity gradient of $-157\,\text{N-unit}\,\text{km}^{-1}$ at the top of ducting layer, corresponding to the location where the largest bending occurs. The Abel inversion used for retrieving refractivity becomes a non-unique inversion problem and result in negative refractivity biases below the ducting layer (Xie et al., 2006), as seen in Figs. 2c and 6. The delta-function like PDF of the RO MRG implies the prevalence of ducting. The systematically smaller MRG in RO refractivity retrieval is primarily caused by the presence of ducting layer at the ABL top.

6.2 Impact of horizontal inhomogeneous atmospheric structure on GPS RO

Over the VOCALS region, the elevated ducting condition is dominant. The idealized 1-D simulation on a horizontally extended ducting layer indicates that the maximum gradients in RO refractivity retrieval should be close to the critical refraction threshold, i.e., $-157\,\text{N-unit}\,\text{km}^{-1}$ (e.g., Sokolovskiy, 2003 and Xie et al., 2006). The maximum bending angle from current COSMIC RO measurements rarely exceeds 0.05 radians, and so the refractivity gradient rarely exceeds $-110\,\text{N-unit}\,\text{km}^{-1}$ over VOCALS region (Fig. 5b). Horizontal averaging of vertical ABL structures by RO can effectively reduce the observed refractivity gradient (e.g., Ao, 2007). In other words, both radiosonde and ECMWF data represent a localized ABL profile, and the ABL height variability may not be uniform over a span of 200 km close to the tangent point, where most GPS RO bending along the ray path is accumulated (Kursinski et al., 1997). Figure 7 clearly shows the deepening of the ABL height in both ECMWF and COSMIC RO. The slope in the ABL heights ($\sim 30\,\text{m}\,100\,\text{km}^{-1}$) indicates the existence of large-scale horizontal inhomogeneity in the atmosphere. Such smoothing effect would need to be further investigated and quantified. Also the 200-m vertical smoothing applied on RO bending profiles further degrades the vertical resolution when sharp bending angle is present.

ACPD
11, 22857–22891, 2011

A more sophisticated filter needs to be developed to preserve the fine structure of the sharp transition in high-resolution bending, which will lead to a larger bending and sharper refractivity gradient at the ABL top.

6.3 Penetration issue and sampling errors

COSMIC RO receivers adopt the open-loop (OL) tracking technique (Sokolovskiy 2001; Ao et al., 2009), which significantly improve the percentage of RO signals to penetrate deep into the lower troposphere. The OL tracking eliminates several problems in previous RO missions (e.g., GPS/MET, CHAMP and GRACE) that use the phase-locked loop (PLL) tracking technique, i.e., early termination of RO signal tracking and systematic tracking errors caused by the complex signal dynamic in the moist lower troposphere (Ao et al., 2003; Beyerle et al., 2003; Anthes et al., 2008). However, the selective lower penetration rate at low latitudes in COSMIC sounding requires further investigation. The improved penetration rate, especially over low latitudes could significantly improve the RO sampling and benefit the science application of GPS RO.

6.4 COSMIC RO ABL height climatology and its implication to model analysis

The difference in the monthly mean ABL height between COSMIC RO and ECMWF analyses (Fig. 7) is substantial and cannot be ignored. Such discrepancy is not caused by the different vertical resolution and the sampling errors in COSMIC RO and could imply the deficiency in model physics. The misrepresentation of MRG and ABL height (Fig. 4) imply incorrect strength and altitude of the inversion layer, which could have profound impact on the entrainment rate and thus cloud evolution simulated in ECMWF models. The climate models with much coarser vertical and horizontal resolution will have even bigger challenge to correctly represent the two critical ABL parameters.

Due to the lack of ABL observations, the state-of-art ABL parameterizations are generally derived and validated by some field campaign observations. The limited spatial and temporal coverage of the measurements could only represent the specific local

ACPD
11, 22857–22891, 2011

physical processes under certain synoptic background forcing conditions. Therefore the fine-tuned parameterization scheme developed from such dataset could potentially biased to certain atmospheric condition and limit its general application in weather and climate models. The global observation of ABL height from COSMIC RO provides an extremely valuable dataset to evaluate various ABL parameterization schemes through the diagnostic analysis.

Soon after its launch in 2006, COSMIC RO soundings have been operationally assimilated into the leading global weather forecasting centers, such as ECMWF and NCEP. Significant positive impacts of RO observations on the upper troposphere and lower stratosphere have been demonstrated (Cucurull et al., 2006; Healy and Thepaut, 2006; Cucurull et al., 2007). However, the much-anticipated positive impact of RO soundings in the lower troposphere, especially over mid and low latitudes has yet to be demonstrated.

NCEP operationally assimilate COSMIC RO refractivity profiles. However, the systematic N-bias in RO refractivity over the subtropics eastern oceans (Xie et al., 2010) along with the complicated error characteristics in the lower troposphere results in very limited impact of RO soundings on model analysis.

ECMWF, on the other hand, assimilate the bending angle, which should not be biased due to ducting. However, in the presence of ducting, RO bending angle loses information inside the ducting layer and a layer right below, and becomes a singularity (e.g., an infinite bending angle) at the top of ducting layer (Sokolovskiy, 2003; Xie et al., 2006). Moreover, directly assimilating RO bending angle in the presence of ducting will not avert the non-unique inversion problem, i.e., a single bending angle corresponds to a continuum of refractivity profiles (Xie et al., 2006). For example, given the constraint of the observed RO bending angle profile, the forward calculation (e.g., computing bending from model refractivity) will not be able to tell the difference among the continuum of model refractivity profiles (including the true and biased profiles). Therefore a better bending and refractivity error covariance need to be developed to better usage of the RO information in the lower troposphere especially in the presence of ducting.

ACPD
11, 22857–22891, 2011

7 Conclusions and future work

In this paper, we analyzed the ABL structures in COSMIC GPS RO, radiosondes and ECMWF analysis data in the SE Pacific where the VOCALS campaign took place. The VOCALS radiosonde observations show well-defined ABL tops with a strong temperature inversion and sharp moisture gradient, which produce a sharp refractivity gradient and a large bending angle in the GPS RO signals. The refractivity gradients over the region are so often large that they exceed critical refraction (e.g., $-157\,\text{N-unit}\,\text{km}^{-1}$) and become ducting (or super-refraction) condition. This situation can result in systematic negative refractivity bias (N-bias) in the standard RO retrieval inside the ABL (Sokolovskiy, 2003; Xie et al., 2006). It is noteworthy that the N-bias seems not affect the ABL height detected with the MRG method. Instead, the very sharp refractivity gradient caused by ducting allows the best detection of ABL height from GPS RO through the simple MRG method.

The comparison of RO ABL height derived from the MRG method with radiosondes is encouraging, whereas ECMWF results show a systematically low bias in the ABL height and the bias become larger in deeper ABL (Fig. 3b). The VOCALS radiosondes exhibit a wide range of ABL height variations ($1 \sim 2$ km) in the PDF, with the peak occurrence frequency at ~1.3 km (Fig. 4b). The vertical smoothing result in slightly lower ABL height with MRG method, but do not change the overall shape of the PDF. The near-coincident COSMIC RO is able to resolve the wide rage of ABL height variations (Fig. 3a, c). ECMWF analysis, on the other hand, tends to produce systematically lower ABL heights as compared with both the near-coincident radiosondes (Fig. 3b) and COSMIC RO soundings (Fig. 3c). The discrepancy between the ECMWF and radiosondes is not caused by the limited vertical resolution (~200 m) in the analysis.

The PDF of radiosonde MRG depends strongly on the vertical resolution of refractivity profile. The higher order smoothing results in a smaller MRG value. All the VOCALS radiosonde data studied here are affected by ducting even after 200-m smoothing. The near-coincident ECMWF analysis (~200-m sampling) underestimates the high MRG

ACPD
11, 22857–22891, 2011

and overestimates the low MRG as compared to radiosondes after 200-m smoothing. On the other hand, COSMIC RO shows systematic bias in the MRG at the ABL top as well as systematic N-bias in RO refractivity inside the ABL, which are primarily caused by the non-unique inversion problem in the presence of ducting. The ABL height derived from COSMIC RO is generally not affected by the ducting layer, however, it would require specific attention for directly using such biased RO refractivity profiles for scientific studies. Simulation study based on radiosonde soundings reveals strong dependence of ducting induced N-bias on vertical resolutions, i.e., higher order smoothing leads to smaller N-bias (Fig. 6). The 100-m smoothing shows peak frequency of N-bias $\sim -12\,\%$, which reduces to $\sim -8\,\%$ with 200-m smoothing and decreases further with additional smoothing. ECMWF analysis shows the PDF of N-bias comparable to close-by radiosonde soundings with ~300-m smoothing, but overestimates the occurrence frequency of non-ducting cases.

Both COSMIC RO and ECMWF analysis clearly show the deepening of the ABL height in the west of the coast of Peru and Chile where ABL varies from shallow stratocumulus topped ABL (~1 km) to much deeper trade wind cumuli. However, the difference in ABL height between ECMWF analysis and COSMIC RO is significant and cannot be ignored. COSMIC RO shows a deeper ABL with a center of minimum ABL height located at (20° S, 75° W), which is located ~10° North of what is seen in ECMWF analysis. The center of the maximum ABL heights (~2.2 km) from COSMIC RO is located 20° west of ECMWF (Fig. 7). The configuration of COSMIC satellites results in significant decrease of RO samples equatorward. Moreover, the RO profiles that penetrate deep into the lowest 500 m of ABL a.m.s.l. also decreases at lower latitudes, which yields even fewer number of valid RO profiles for ABL studies at low latitudes. The sampling error due to the limited COSMIC RO sampling is estimated to be generally small for the nine-month composite, but could become significant for shorter period especially over low latitudes.

The ABL height observed from COSMIC RO provides a valuable dataset for diagnosing analysis of various ABL parameterization schemes in weather and climate models.

ACPD
11, 22857–22891, 2011

The biased RO refractivity due to ducting over the eastern oceans and the trade wind regions (Xie et al., 2010) would need to be corrected (e.g., Xie et al., 2006) before scientific application. Improving penetration rate of RO soundings in the ABL over low latitudes and a better understanding of horizontal averaging effect by RO would further enhance the scientific values of RO soundings for global ABL studies.

Acknowledgements. This work was supported by an appointment to JIFRESSE at UCLA. F. Xie and E. R. Kursinski are partly supported by NOAA JCSDA. D. L. Wu, C. O. Ao and A. J. Mannucci are supported by the Jet Propulsion Laboratory (JPL), California Institute of Technology, under contract with the National Aeronautics and Space Administration (NASA). The COSMIC RO soundings are provided by JPL. The VOCALS radiosondes were provided by NCAR/EOL under sponsorship of the National Science Foundation. The high-resolution YOTC (Year of Tropical Convection) analyses were provided by ECMWF. The authors would like to thank Byron Iijima, Marc Pestana for assistance with the COSMIC retrievals and Evan Fishbein at JPL for help with ECMWF data.

References

Anthes, R. A., Bernhardt, P. A., Chen, Y., Cucurull, L., Dymond, K. F., Ector, D., Healy, S. B., Ho, S.-P., Hunt, D. C., Kuo, Y.-H., Liu, H., Manning, K., McCormick, C., Meehan, T. K., Randel, W. J., Rocken, C., Schreiner, W. S., Sokolovskiy, S. V., Syndergaard, S., Thompson, D. C., Trenberth, K. E., Wee, T.-K., Yen, N. L., and Zeng, Z.: The COSMIC/FORMOSAT-3 mission: Early results, B. Am. Meteorol. Soc., 89, 313–333, 2008.

Ao, C. O.: Effect of ducting on radio occultation measurements: An assessment based on high-resolution radiosonde soundings, Radio Sci., 42, RS2008, doi:10.1029/2006RS003485, 2007.

Ao, C. O., Meehan, T. K., Hajj, G. A., Mannucci, A. J., and Beyerle, G.: Lower-troposphere refractivity bias in GPS occultation retrievals, J. Geophys. Res., 108, 4577, doi:10.1029/2002JD003216, 2003.

Ao, C. O., Chan, T. K., Iijima, B. A., Li, J.-L., Mannucci, A. J., Teixeira, T., Tian, B., and Waliser, D. E.: Planetary boundary layer information from GPS radio occultation measurements,

ACPD

11, 22857–22891, 2011

ECMWF GRAS SAF Workshop on Applicaitons of GPS Radio Occultation Measurements (16–18 June 2008), Reading, UK, 123–131, 2008.
Ao, C. O., Hajj, G. A., Meehan, T. K., Dong, D., Iijima, B. A., Mannucci, A. J., and Kursinski, E. R.: Rising and setting GPS occultations by use of open-loop tracking, J. Geophys. Res., 114, D04101, doi:10.1029/2008JD010483, 2009.
Basha, G. and Ratnam, M. V.: Identification of atmospheric boundary layer height over a tropical station using high resolution radiosonde refractivity profiles: Comparison with GPS radio occultation measurements, J. Geophys. Res., 114, D16101, doi:10.1029/2008JD011692, 2009.
Bauer, P., Lopez, P., Benedetti, A., Salmond, D., and Moreau, E.: Implementation of 1D+4D-Var assimilation of precipitation affected microwave radiances at ECMWF, Part I: 1D-Var, Q. J. Roy. Meteor. Soc., 132, 2277–2306, 2006.
Beyerle, G., Schmidt, T., Wickert, J., Heise, S., Rothacher, M., König-Langlo, G., and Lauritsen, K. B.: Observations and simulations of receiver-induced refractivity biases in GPS radio occultation, J. Geophys. Res., 111, D12101, doi:10.1029/2005JD006673, 2006.
Bony, S. and Dufresne J.-L.: Marine boundary layer clouds at the heart of tropical cloud feedback uncertainties in climate models, Geophys. Res. Lett., 32, L20806, doi:10.1029/2005GL023851, 2005.
Bretherton, C. S., Uttal, T., Fairall, C. W., Yuter, S. E., Weller, R. A., Baumgardner, D., Comstock, K., Wood, R., and Raga, G. B.: The EPIC 2001 stratocumulus study, B. Am. Meteorol. Soc., 85, 967–977, doi:10.1175/BAMS-85-7-967, 2004.
Bretherton, C. S., Wood, R., George, R. C., Leon, D., Allen, G., and Zheng, X.: Southeast Pacific stratocumulus clouds, precipitation and boundary layer structure sampled along 20° S during VOCALS-REx, Atmos. Chem. Phys., 10, 10639–10654, doi:10.5194/acp-10-10639-2010, 2010.
Clement, A. C., Burgman R., and Norris J. R.: Observational and model evidence for positive low-level cloud feedback, Science, 325, 460–464, doi:10.1126/science.1171255, 2009.
Cucurull, L., Kuo, Y. H., Barker, D., and Rizvi, S. R. H.: Assessing the impact of simulated COSMIC GPS radio occultation data on weather analysis over the Antarctic: A case study, Mon. Weather Rev., 134, 3283–3296, 2006.
Cucurull, L., Derber, J. C., Treadon, R., and Purser, R. J.: Assimilation of Global Positioning System radio occultation observations into NCEP's Global Data Assimilation System, Mon. Weather Rev., 135, 3174–3193, 2007.

ACPD
11, 22857–22891, 2011

Deardorff J. W.: On the entrainment rate of a stratocumulus-topped mixed layer, Q. J. Roy. Meteor. Soc., 102, 563–582, 1976.
Fjeldbo, G., Kliore, A. J., and Eshleman, V. R.: The neutral atmosphere of Venus as studied with the Mariner V radio occultation experiment, Astron. J., 76, 123–140, 1971.
Gorbunov, M. E., Benzon, H.-H., Jensen, A. S., Lohmann, M. S., and Nielsen, A. S.: Comparative analysis of radio occultation processing approaches based on Fourier integral operators, Radio Sci., 39, RS6004, doi:10.1029/2003RS002916, 2004.
Hajj, G. A., Kursinski, E. R., Romans, L. J., Bertiger, W. I., and Leroy, S. S.: A technical description of atmospheric sounding by GPS occultationm, J. Atmos. Sol.-Terr. Phy., 64, 451–469, 2002.
Healy, S. and Thépaut, J.-N.: Assimilation experiments with CHAMP GPS radio occultation measurements, Q. J. Roy. Meteor. Soc., 132, 605–623, 2006.
Jordan, N. S., Hoff, R. M., and Bacmeister, J. T.: Validation of Goddard Earth Observing System-version 5 MERRA planetary boundary layer heights using CALIPSO, J. Geophys. Res., 115, D24218, doi:10.1029/2009JD013777, 2010.
Klein, S. A. and Hartmann, D. L.: The seasonal cycle of low stratiform clouds, J. Climate, 6, 1587–1606, 1993.
Kursinski, E. R., Hajj, G. A., Schofield, J. T., Linfield, R. P., and Hardy, K. R.: Observing Earth's atmosphere with radio occultation measurements using the Global Positioning System, J. Geophys. Res., 102, 23429–23465, 1997.
Lilly, D. K.: Models of cloud topped mixed layers under a strong inversion, Q. J. Roy. Meteor. Soc., 94, 292–309, 1968.
Lopez P.: A 5-yr 40-km-Resolution Global Climatology of Superrefraction for Ground-Based Weather Radars, J. Appl. Meteorol. Clim., 48(1), 89–110, 2009.
Ma, C.-C., Mechoso, C. R., Robertson, A. W., and Arakawa, A.: Peruvian stratus clouds and the tropical Pacific circulation: A coupled ocean-atmosphere GCM study, J. Climate, 9, 1635–1645, 1996.
Palm, S. P., Benedetti, A., and Spinhirne, J.: Validation of ECMWF global forecast model parameters using GLAS atmospheric channel measurements, Geophys. Res. Lett., 32, L22S09, doi:10.1029/2005GL023535, 2005.
Poli, P., Healy, S. B., and Dee, D. P.: Assimilation of global positioning system ratio occultation data in the ECMWF ERA-Interim reanalysis, Q. J. Roy. Meteor. Soc., 136, 1972–1990, doi:10.1002/qj.722, 2010.

ACPD
11, 22857–22891, 2011

Randall, D. A., Coakley, J. A., Lenschow, D. H., Fairall, C. W., and Kropfli, R. A.: Outlook for Research on Subtropical Marine Stratification Clouds, B. Am. Meteorol. Soc., 65, 1290–1301, 1984.

Randall, D., Curry, J., Battisti, D., Flato, G., Grumbine, R., Hakkinen, S., Martinson, D., Preller, R., Walsh, J., and Weatherly, J.,: Status and outlook for large scale modeling of atmosphere-ice-ocean interactions in the Arctic. Bull. Am. Met. Soc., 79, 197–219, 1998.

Seidel D., Ao, C. O., and Li, K.: Estimating climatological planetary boundary layer heights from radiosonde observations: Comparison of methods and uncertainty analysis, J. Geophys. Res., doi:10.1029/2009JD013680, 2010.

Slingo, A.: Sensitivity of the earth's radiation budget to changes in the low clouds, Nature, 343, 49–51, 1990.

Smith, E. K. and Weintraub, S.: The constants in the equation for atmospheric refractive index at radio frequencies, Proc. Inst. Radio Engrs., 41, 1035–1037, 1953.

Sokolovskiy, S. V.: Tracking tropospheric radio occultation signals from low Earth orbit, Radio Sci., 36, 483–498, 2001.

Sokolovskiy, S. V.: Effect of superrefraction on inversions of radio occultation signals in the lower troposphere, Radio Sci., 38, 1058, doi:10.1029/2002RS002728, 2003.

Sokolovskiy, S., Kuo, Y.-H., Rocken, C., Schreiner, W. S., Hunt, D., and Anthes, R. A.: Monitoring the atmospheric boundary layer by GPS radio occultation signals recorded in the open-loop mode, Geophys. Res. Lett., 33, L12813, doi:10.1029/2006GL025955, 2006.

Sokolovskiy, S. V., Rocken, C., Lenschow, D. H., Kuo, Y.-H., Anthes, R. A., Schreiner, W. S., and Hunt, D. C.: Observing the moist troposphere with radio occultation signals from COSMIC, Geophys. Res. Lett., 34, L18802, doi:10.1029/2007GL030458, 2007.

von Engeln, A. and Teixeira, J.: A ducting climatology derived from the European Centre for Medium-Range Weather Forecasts global analysis fields, J. Geophys. Res., 109, D18104, doi:10.1029/2003JD004380, 2004.

von Engeln, A. and Teixeira J.: A planetary boundary layer height climatology derived from ECMWF Re-analysis data, J. Appl. Meteorol. Clim., submitted, 2011.

Wang, J., Rossow, W. B., Uttal, T., and Rozendaal, M.: Variability of cloud vertical structure during ASTEX observed from a combination of rawinsonde, radar, ceilometer and satellite, Mon. Weather Rev., 127, 2484–2502, 1999.

Wood, R. and Bretherton, C. S.: Boundary layer depth, entrainment and decoupling in the cloud-capped subtropical and tropical marine boundary layer, J. Climate, 17, 3576–3588,

ACPD
11, 22857–22891, 2011

2004.
Wood, R., Mechoso, C. R., Bretherton, C. S., Weller, R. A., Huebert, B., Straneo, F., Albrecht, B. A., Coe, H., Allen, G., Vaughan, G., Daum, P., Fairall, C., Chand, D., Gallardo Klenner, L., Garreaud, R., Grados, C., Covert, D. S., Bates, T. S., Krejci, R., Russell, L. M., de Szoeke, S., Brewer, A., Yuter, S. E., Springston, S. R., Chaigneau, A., Toniazzo, T., Minnis, P., Palikonda, R., Abel, S. J., Brown, W. O. J., Williams, S., Fochesatto, J., Brioude, J., and Bower, K. N.: The VAMOS Ocean-Cloud-Atmosphere-Land Study Regional Experiment (VOCALS-REx): goals, platforms, and field operations, Atmos. Chem. Phys., 11, 627–654, doi:10.5194/acp-11-627-2011, 2011.
Xie, F.: Development of a GPS Occultation Retrieval Method for Characterizing the Marine Boundary Layer in the Presence of Super-refraction, Dissertation, University of Arizona, 134 pp., 2006.
Xie, F., Syndergaard, S., Kursinski, E. R., and Herman, B. M.: An Approach for Retrieving Marine Boundary Layer Refractivity from GPS Occultation Data in the Presence of Super-refraction, J. Atmos. Ocean. Tech., 23, 1629–1644, 2006.
Xie, F., Wu, D. L., Ao, C. O., Kursinski, E. R., Mannucci, A., and Syndergaard, S.: Super-refraction effects on GPS radio occultation refractivity in marine boundary layers, Geophys. Res. Lett., 37, L11805, doi:10.1029/2010GL043299, 2010.
Zeng, X., Brunke, M. A., Zhou, M., Fairall, C., Bond, N. A., and Lenschow, D. H.: Marine atmospheric boundary layer height over the eastern Pacific: data analysis and model evaluation, J. Climate, 17, 4159–4170, 2004.

ACPD
11, 22857–22891, 2011

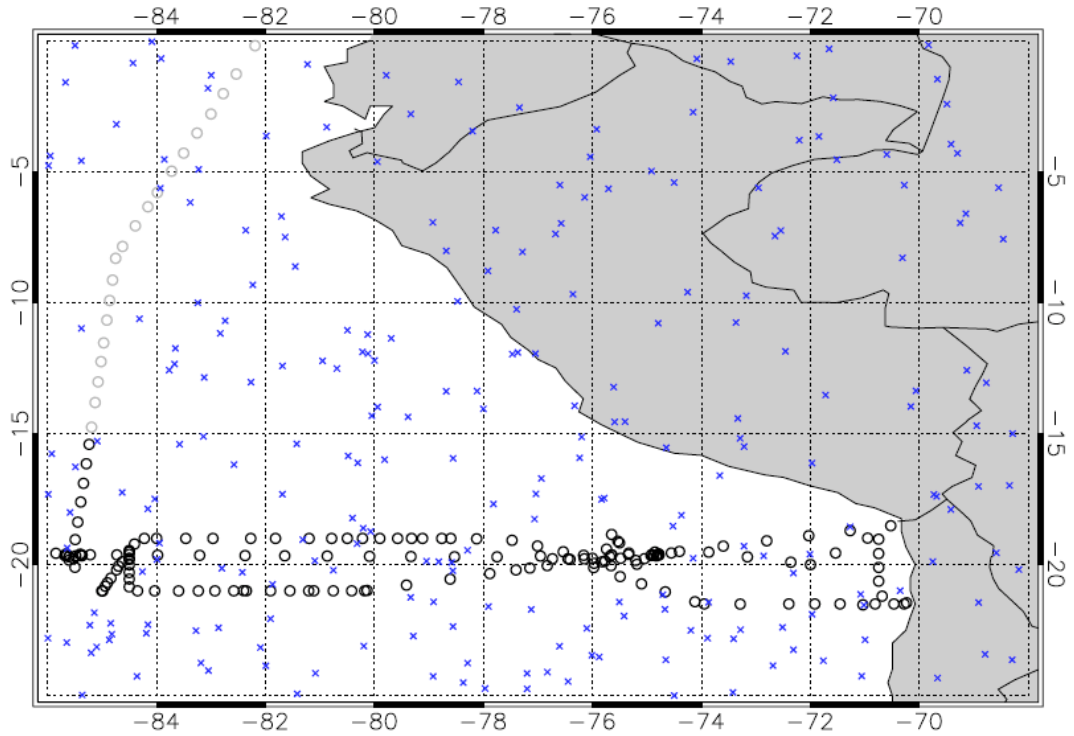

Fig. 1. Map of the ship-borne radiosonde (circle) and COSMIC RO sounding locations (cross) during VOCALS – Rex field campaign from 20 October to 1 December 2008.

ACPD
11, 22857–22891, 2011

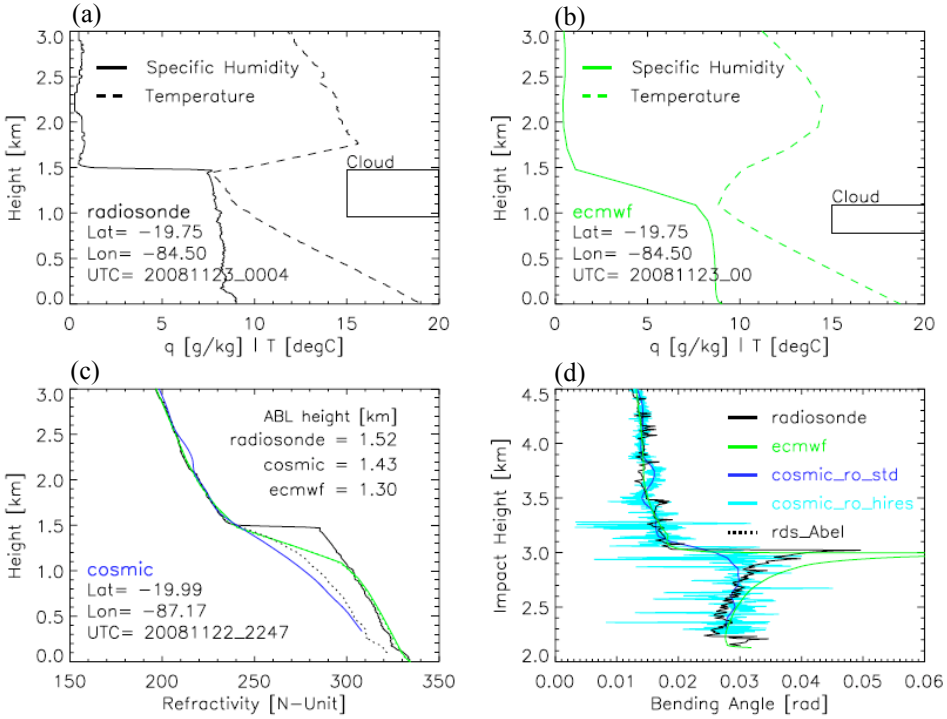

Fig. 2. Typical ABL structure in one VOCALS radiosonde (black) with the near-coincident COSMIC-RO (blue) and ECMWF analysis (green) profiles. **(a)** Radiosonde specific humidity and temperature; **(b)** ECMWF analysis specific humidity and temperature; The boxes in **(a, b)** indicates the cloud region with relative humidity exceeding 94 %; **(c)** refractivity of radiosonde (black), COSMIC RO (blue) and ECMWF analysis (green) as well as simulated refractivity retrieval (black-dotted) based on the simulated radiosonde bending; the ABL heights are listed in the upper right corner, respectively; **(d)** simulated bending angle of radiosonde (black) and ECMWF analysis (green) as well as the standard (blue-solid) and high-resolution (cyan) COSMIC RO bending angles.

ACPD
11, 22857–22891, 2011

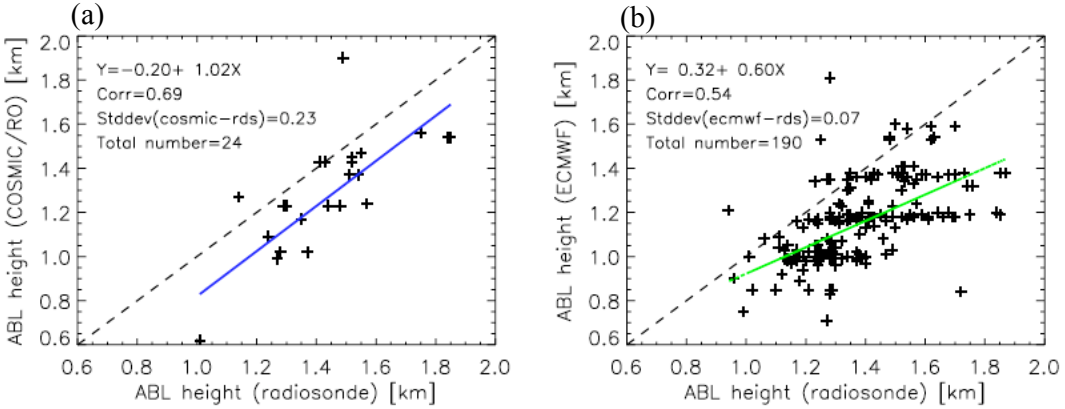

Fig. 3. (a) scatter-plot of ABL height of radiosonde (100-m smoothing) and the near-coincident COSMIC RO soundings (plus) with the linear fit (blue-solid); **(b)** scatter-plot of ABL height for collocated radiosonde and ECMWF analysis (plus) with the linear fit (green-solid).

ACPD
11, 22857–22891, 2011

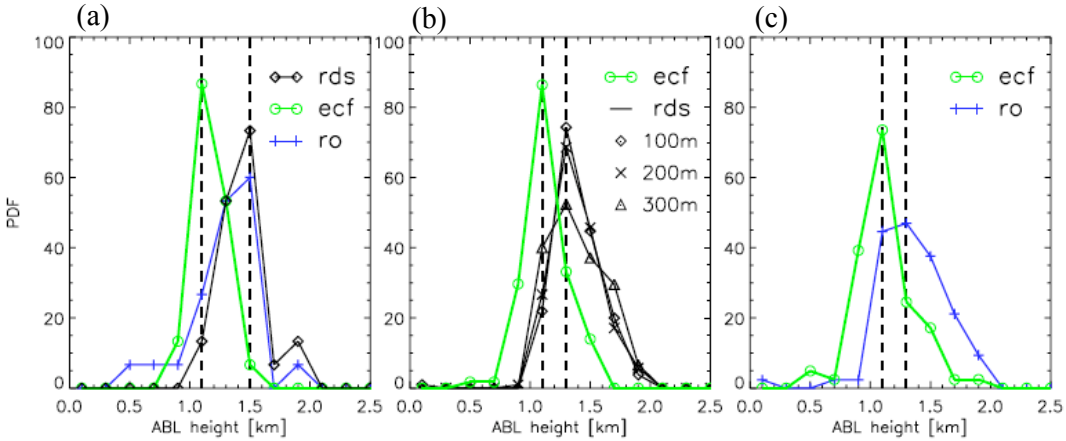

Fig. 4. The PDF of ABL heights **(a)** for radiosondes (25 profiles, with 100-m smoothing), the near-coincident COSMIC RO and ECMWF analysis; **(b)** for radiosonde soundings (190 profiles) with three vertical smoothing intervals (100, 200 and 300 m) and the near-coincident ECMWF analysis over the region (latitudes: 15° S–25° S, longitudes: 70° W–86° W) from 25 October to 1 December; **(c)** for COSMIC RO soundings (70 profiles) and the near-coincident ECMWF analysis over the region (latitudes: 20° S–25° S, longitudes: 70° W–86° W) from 25 October to 1 December. For better illustration, the normalized PDF is divided by 3 to scale the maximum PDF close to 100. The shape of the PDF is not changed due to the scaling.

ACPD
11, 22857–22891, 2011

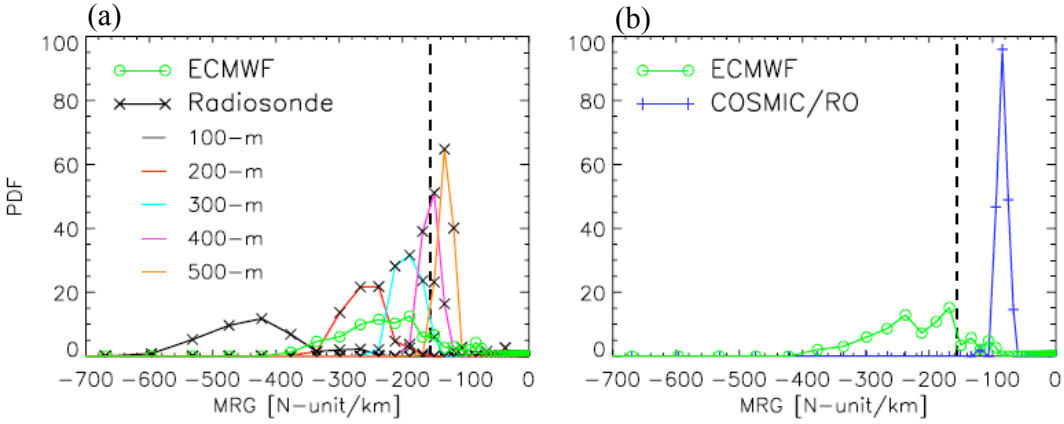

Fig. 5. **(a)** PDF of MRG for the radiosondes (190 profiles, with different vertical smoothing) and the near-coincident ECMWF analysis over the region (latitudes: 15° S–25° S, longitudes: 70° W–86° W); **(b)** PDF of the MRG for COSMIC RO soundings (70 profiles) and the near-coincident ECMWF analysis over the region (latitudes: 20° S–25° S, longitudes: 70° W–86° W) from 25 October to 1 December. The vertical black dashed lines denote the critical refraction gradient (-157 N-unit km^{-1}). The normalized PDF is multiplied by 20 for better illustration.

ACPD
11, 22857–22891, 2011

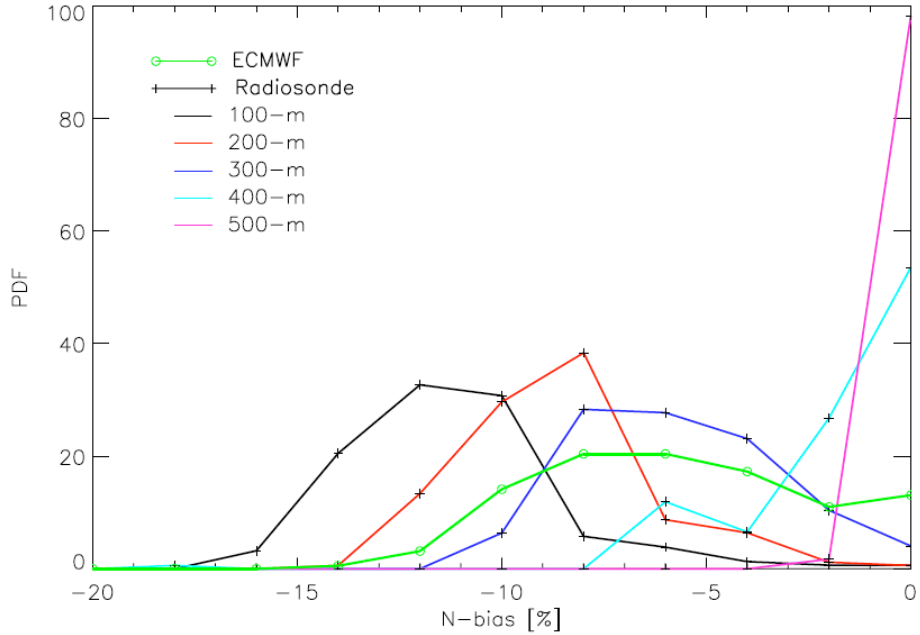

Fig. 6. PDF of the maximum N-bias due to ducting for radiosondes (190 profiles, with different vertical smoothing) and the near-coincident ECMWF analysis over the region (latitudes: 15° S–25° S, longitudes: 70° W–86° W). The normalized PDF is multiplied by 2 to scale the maximum PDF close to 100.

ACPD
11, 22857–22891, 2011

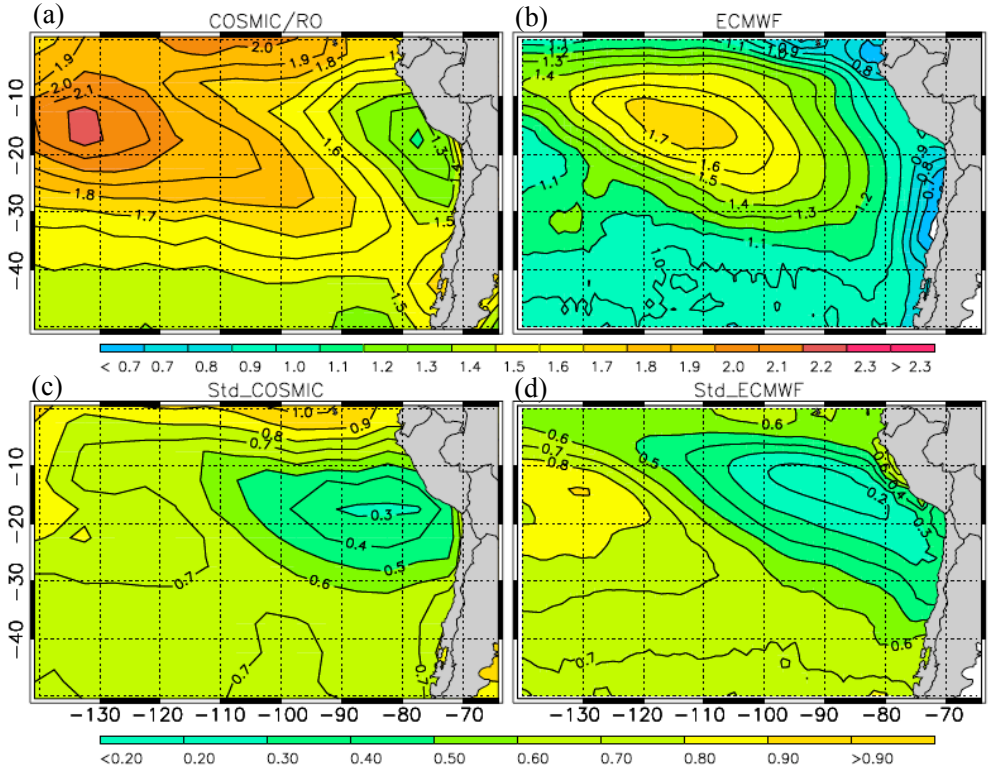

Fig. 7. Mean climatology (September to November from 2007 to 2009) of ABL heights derived from **(a)** COSMIC RO and **(b)** ECMWF analysis. The standard deviation of the ABL heights is shown in **(c)** and **(d)**, respectively.

ACPD
11, 22857–22891, 2011

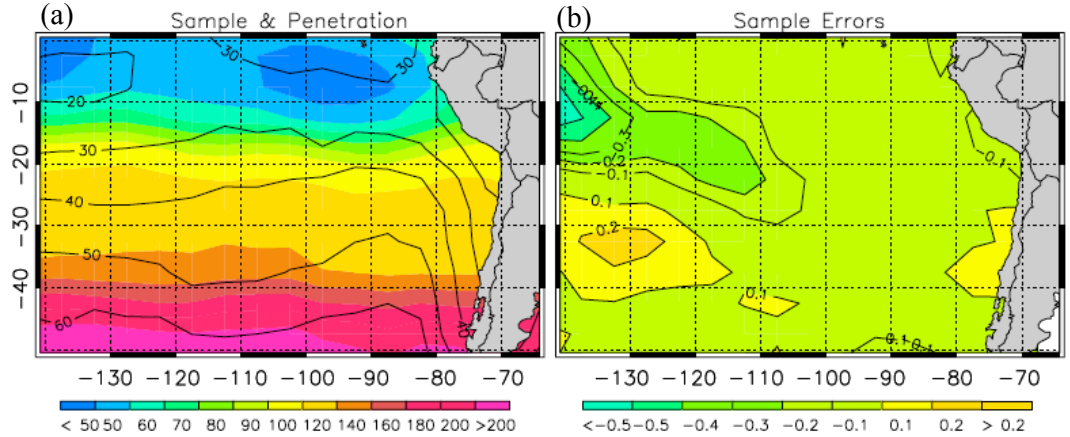

Fig. 8. **(a)** Number of COSMIC RO soundings per area of 500 × 500 km (shaded); the overplotted contours denote the percentage of soundings that penetrate below 500 m a.m.s.l.; **(b)** errors in ABL heights caused by the limited COSMIC RO sampling derived from ECMWF analysis (contours, with 0.1 km interval).

ACPD
11, 22857–22891, 2011